Fabrication of Dense Aluminum Nanoparticle Arrays with Controllable Deep Ultraviolet Surface Plasmon Resonance Properties

Y Y Ding, G Xu, J A Chen, F Liu and M Han *

National Laboratory of Solid State Microstructures, Department of Materials Science and Engineering, and Collaborative Innovation Centre of Advanced Microstructures, Nanjing University, Nanjing 210093, China

Corresponding author and e-mail: M Han, sjhanmin@nju.edu.cn

Abstract. UV irradiation was used to tailor the surface plasmon band of the densely distributed Al nanoparticle arrays fabricated by gas phase deposition. We showed that the broad surface plasmon resonance band of the as-prepared sample could be tuned to a sharp and strong resonance band in the DUV optical range, with a large blue shift of the peak wavelength. The evolution of the surface plasmon resonance properties was attributed to the UV irradiation-improved surface oxidation of the nanoparticles, which vanished the nearfield couplings between the closely spaced nanoparticles by increasing their interspacing.

1. Introduction

Aluminium nanoparticles (Al NPs) are of interest to a variety of applications, such as photocatalysts [1], optical coatings [2], transparent conductive films [3], as well as propellant and explosive materials [4]. They have been receiving considerable interest lately as plasmonic materials alternative to gold and silver NPs, with their attractive properties such as low cost, high natural abundance, and advantages in device performance, design flexibility, processing and tenability [5-11]. Al NPs are especially attractive for UV plasmonics because they exhibit surface plasmon resonance (SPR) properties in the full UV range. Particularly, the SPR of small Al NPs locates in the deep ultraviolet (DUV) region of the optical spectrum, which is of great interest in numerous applications; e.g. ultrasensitive organic molecule sensing [5, 6] and photocatalysis[7,8]. Short wavelength UV light is capable of breaking organic bonds, which is the key to biological applications.

The surface plasmons (SPs) of Al NPs and their assemblies are extremely sensitive to the geometrical characteristics [9, 12-14]. The SPR bands can be tuned in a wide spectrum range from the DUV to the IR by varying the particle size, shape as well as the inter-particle spacing. For an individual Al NP, the SPR wavelength increases with its diameter D and reaches 300 nm at D=70 nm[9], which means it is difficult to generate SPR at DUV wavelengths with Al NPs fabricated with standard lithography techniques[15]. For NPs prepared by various bottom-up synthetic methods, the distribution in particle size and impurities induce broadened or even featureless SPR spectra. The

Ding, Y., Xu, G., Chen, J., Liu, F. and Han, M.
Fabrication of Dense Aluminum Nanoparticle Arrays with Controllable Deep Ultraviolet Surface Plasmon Resonance Properties.
In *Proceedings of the International Workshop on Materials, Chemistry and Engineering (IWMCE 2018)*, pages 591-597
ISBN: 978-989-758-346-9

impact of oxidation is huge to the smaller NPs, which are concerned majorly in DUV applications. Furthermore, aggregation of the NPs in the dense array induces large red-shift and broadening of the SPR bands due to the nearfield coupling among the closely spaced NPs. Therefore challenges still remain to synthesize well-controlled Al NPs suitable for DUV plasmonic applications.

As a poor metal, aluminium is easily oxidized when expose to the atmosphere. A thin native oxide layer can be formed on the surface so that the Al NP is wrapped with a shell. The formation of alumina layer is an important property. It acts as a passivation layer and prevents further oxidation of the Al NPs. As a result, highly stable and discrete Al NPs can ultimately be prepared. Furthermore, the SPR of the Al NPs also depends sensitively on the presence of the dielectric oxide shell [16,17]. Consequently, oxidation can be a means to tune the SPR of the Al NPs by controllable growth of the dielectric shell. In this paper we report the evolution of the UV SPR bands of the densely distributed Al NPs induced by surface oxidation assisted by UV light irradiation. We show that the UV irradiation can sufficiently tune the SP spectra of the gas-phase synthesized Al NP arrays into a sharp and strong resonance in the DUV optical range.

2. Materials and methods

2.1. Preparation of Al NPs.

We used a magnetron gas aggregation cluster source [18] to generate Al NPs in gas phase. Atoms were sputtered from the Al target and Al clusters were formed through the aggregation process in the argon gas. A stable argon gas flow was introduced into the liquid nitrogen cooled aggregation tube to maintain a constant carrier gas pressure for cluster growth. The cluster size was controlled by the carrier gas pressure. The clusters were swept by the gas stream into a high vacuum chamber through a nozzle and deposited on the UV-grade fused silica substrate surface.

2.2. Characterization and optical measurements.

The size and morphology of the Al NPs was characterized with a transmission electron microscope (TEM). The extinction spectra of the Al NP arrays are collected in a transmission configuration using a UV-vis spectrophotometer equipped with a deuterium lamp light source. The measurement was performed at normal incidence.

3. Results and discussion

Figure 1 shows the TEM image of the Al NPs prepared under argon gas pressure of 50 Pa. As shown in the figure, the Al NPs distributed on the substrate surface randomly and aggregations occurred among most of the particles. The average diameter of the NPs was measured to be 19 nm, with a size distribution of about 6 nm.

Figure 2 shows an extinction spectrum of the Al NP arrays collected in a transmission configuration using a UV-vis spectrophotometer equipped with a deuterium lamp light source. The measurement was performed at normal incidence. The spectrum is dominated by a very broad resonance peak, covering the wavelength range from about 210 nm to longer than 400 nm. The peak wavelength is about 270 nm. The spectrum displayed little change when measured following several days of atmospheric exposure, implying that the NPs were passivated effectively with the self-terminating native Al oxide. Also shown in Figure 2 is the extinction coefficient for an individual 14 nm Al sphere encapsulated with a 3 nm oxide shell calculated using the finite difference time domain (FDTD) method. Significant discrepancies appear when comparing the experimental and calculated spectrum. The experimental spectrum displays a large red-shift (>60 nm) and becomes very broadened. Its shape also departures from the characteristic Lorentzian resonance of a dipolar oscillator.For small Al NPs, the SPR bands redshift with increasing particle diameter, so that the size

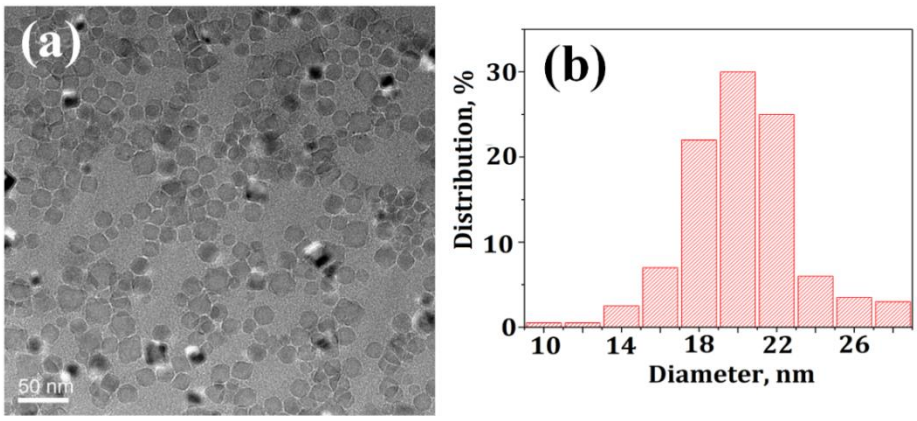

Figure 1. (a) TEM image of Al NPs generated with cluster beam deposition. (b) Histogram measured from the TEM images.

distribution exists in the NP arrays may induce SPR band broadening. However the size distribution-induced broadening should not dominate the experimental spectrum since only less than 25 nm red-shift could be expected [19] when the size of the NP changes from 15 nm to 25 nm, a size region which includes most of the Al NPs. We thus attribute the red-shift and broadening of the experimental spectrum observed herein to the near field couplings occurr among the closely spaced NPs in the dense arrays. It has been reported that the near-field couplings between NPs in close proximity will not only broaden the resonant peak but also red-shift the resonant wavelength [20]. The fractional plasmon red-shift ($\Delta\lambda/\lambda$, where λ denotes the SPR wavelength and $\Delta\lambda$ is the red-shift induced by near-field coupling) decays near-exponentially over a ratio of inter-particle spacing S/D, that is [21]: $\Delta\lambda/\lambda \sim \exp(-K\,S/D)$, where K is a constant. This means shorter interparticle spacing permits much stronger nearfield coupling, which generates a larger red-shift. Previous research showed [22] that in the dense array of 8 nm sized Ag NPs generated by cluster beam deposition, with the increase of the NP density the SPR wavelength demonstrated a redshift from less than 400 nm to more than 570 nm, in accompanying with an increased broadening of the resonance peak. Although near-field coupling could sufficiently tune the SPR bands in a wide wavelength region, which will be important for many applications[13,15], for DUV plasmonics the red-shift and broadening of the SPR band will be failed to satisfy the practical application conditions, especially when a high density of NPs is required to provide sufficient enhancement.

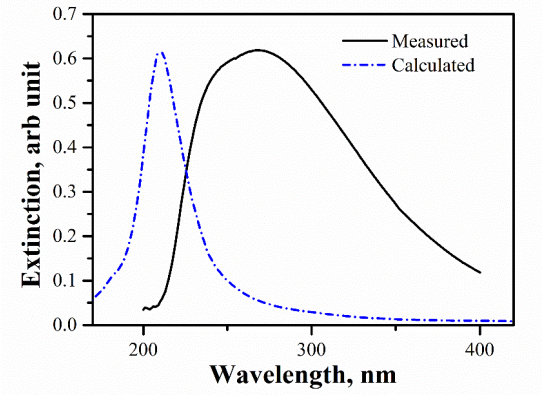

Figure 2. Experimental extinction spectrum (solid) of the Al NP arrays, normalized to the bare fused silica substrate, and the calculated extinction coefficient (dashed line) of an individual 14 nm Al NP coated with a 3 nm oxide shell.

We found that the SPR band of the Al NP arrays could be tailored by UV light irradiation. To exam this, the Al NP samples were attached on the rotatable sample stage of the UV-vis spectrophotometer equipped with a 30 W deuterium lamp light source. Real-time extinction spectra were collected in a transmission configuration at room temperature every 5 minutes for holding times up to 140 min. Meanwhile, the NPs were exposed to the UV illumination of the deuterium lamp continuously. Shown in Figure 3 are representative extinction spectra recorded during UV irradiation.

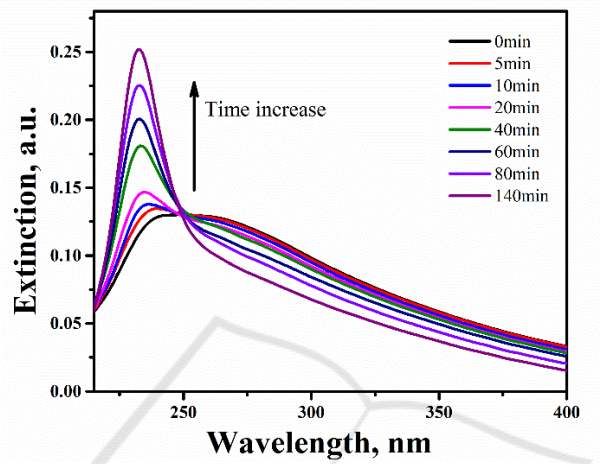

Figure 3. Extinction spectra of the Al NP arrays recorded in real time during UV irradiation in air at room temperature. Total holding time **is** 140min.

With UV irradiation, a sharp extinction band between 220 and 250 nm rose at the shorter wavelength edge of the original broad band, in accompanying with a continuous decrease in the extinction peak intensity at longer wavelength. The new extinction band became more and more intense with the increase of the UV irradiation time. The new band peaked at 240 nm with 5 min irradiation, and monotonously shifted to shorter wavelength when increasing the UV exposure time. Also evident was the continuous narrowing of the extinction band. With 140min UV irradiation, the original broad SPR band almost vanished, remaining a sharp intense SPR band peaks at 232 nm, with a full width at half maximum (FWHM) of about 20 nm.

The evolution of the SPR band in Al NP arrays under UV irradiation might be attributed to the growth of the oxide layers on the NP surfaces inspired by UV light. The change on the oxide shell thickness of the NPs varied both the size and interspacing of the NPs. In Figure 3, the broad band in longer wavelength was attributed to the near-field coupled SPs of closely spaced Al NPs, while the new arisen sharp band in shorter wavelength DUV region could be attributed to the intrinsic SPs of the isolated Al NPs. UV irradiation induced thicker Al oxide layers, which increased the interspacing and vanished the nearfield couplings between them. With the increase of the oxide shell thickness, the proportion of the isolated NPs became larger, which resulted in the pronounced shorter wavelength SPR band that corresponded to the isolated Al NPs. On the other hand, the SPR wavelength of an isolated Al NP depended sensitively on the presence of the oxide shell on its surface. The variation caused by NP oxidation depended on two factors, which generated opposite changes: the reduction of the metallic core size leaded to a blue shift and narrowing of the SPR band, whereas an increase of the effective refractive index surrounding the core resulted in a red shift and broadening of the SPR band. For smaller Al NPs, as the oxide shell increased, the blue-shift and sharping compensated and dominated the red-shift and broadening [10, 17]. Therefore, the results on

the time evolution of the SPR for the Al NP arrays under UV irradiation appeared consistent with the trends predicted with the above analysis, i.e., the rising of the DUV SPR band, and the FWHM decrease and blue shift of its peak.

The increase of the oxide shell thickness of the Al NPs under UV irradiation can also be verified with high resolution TEM (HRTEM). Figure 4(a)-(c) shows HRTEM images of three individual Al NPs with different diameters (D = 15, 23 and 40 nm). Prior to the HRTEM observation the NPs had been exposed to UV irradiation in atmospheric ambient for 140min. From these images, spherically shaped core/shell nanoparticles could be clearly observed. Lattice images were distinguished in the cores, implying they were Al nanocrystals. We believed that the amorphous shells were most likely Al_2O_3. Although the oxide shell was not very uniform for each individual Al NPs, its thickness kept around 6 nm on average and did not vary with the NP size. It should be noted that the oxide layer observed here was considerable thicker than those reported for small Al particles previously (typically 2.5 nm) [23, 24]. In Figure 4(d), a HRTEM image of an individual Al NP without UV irradiation is also shown. The sample had been exposed to atmospheric ambient for four days before the observation. Comparing with the NPs shown in Figure 4(a)-(c), its oxide shell was much thinner and obscure.

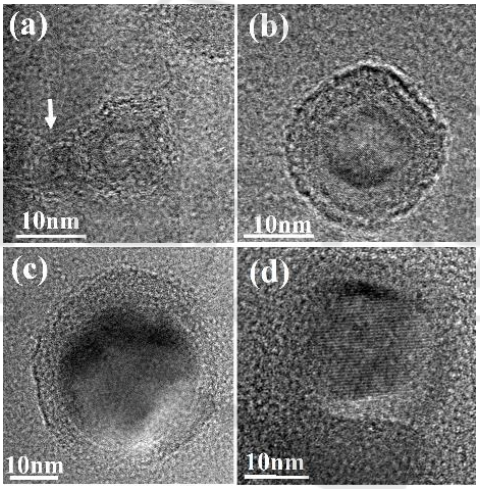

Figure 4.(a)-(c) HRTEM images of individual UV exposed Al NPs with different sizes, (a) D = 15 nm, (b) D=23 nm, (c) D= 40 nm, respectively. (d) HRTEM image of an individual Al NP without UV exposing.

Figure 5 shows the extinction coefficient of two closely touched 20 nm Al nanoparticles using FDTD method, where t represents the thickness of the oxide shell on the surface of the nanoparticles. When t=0, two Al nanoparticles are in contact, resulting in a wide band that extends to over 400nm at the long wavelength due to near-field coupling. When two nanoparticles have the oxide layer, the wide extinction band at the long wavelength disappears, while a sharp extinction peak appears at the wavelength below 250 nm. With the thickening of the oxide layer, the extinction peak further blue shifts .This calculation is in line with the previous experimental results.

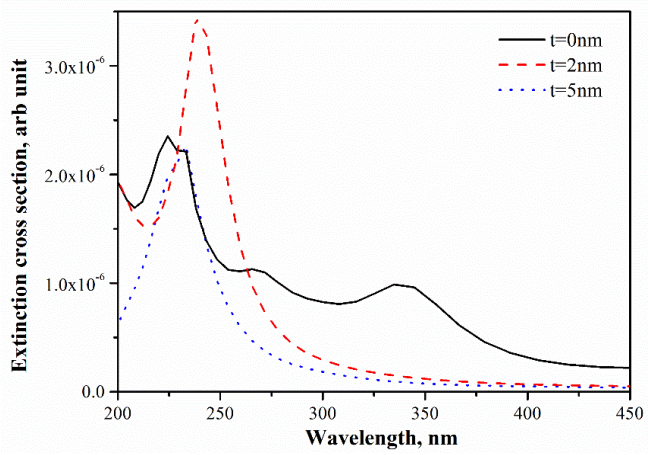

Figure 5. Extinction coefficient of two closely touched 20nm Al nanoparticles with different surface oxide shell thickness.

4. Conclusions

In summary, we have fabricated dense arrays of Al NPs with an average size of about 19 nm by the gas phase cluster beam deposition method. The NP arrays exhibited broad SPR spectra in the UV region, owing to the red-shift induced by the near field couplings between the closely spaced nanoparticles. UV irradiation have been used to tailor the plasmonic properties in Al NP arrays. We have shown that the UV irradiation induced a large blue shift of the SPR band, resulted in a sharp and strong SPR band in the DUV region, peaked at 232 nm with a FWHM of 20nm. The evolution of the SPR property was attributed to the growth of the oxide shells on the NP surfaces inspired by UV light, which vanished the near-field couplings between the closely spaced Al NPs by increase their interspacing. The increase of the oxide shell thickness of the Al NPs under UV irradiation has been verified by HRTEM. We have demonstrated an easy way to realize intense DUV SPR in stable Al NP arrays, which might find broad applications, such as ultraviolet Raman spectroscopy, sensing, and photovoltaics.

Acknowledgments

We thank the financial support from the National Natural Science Foundation of China (Grant nos. 11627806, 11604161, 61301015), the National Basic Research Programme of China (973 Program, Grant nos. 2014CB932302). This research was also supported by a project funded by the Priority Academic Programme Development of Jiangsu Higher Education Institutions.

References

[1] Zhou L, Zhang C, McClain M, Manjavacas A, Krauter C, Tian S, Erg F B, Everitt H, Carter E, Nordlander P and Halas N 2016 Aluminum nanocrystal as a plasmonic photocatalyst for hydrogen dissociation *Nano Lett.* **16** 1478-84

[2] Lachebi I, Fedala A, Djenizian T, Hadjersi T and Kechouane M 2018 Morphological and optical properties of aluminum nanoparticles deposited by thermal evaporation on heated substrates *Surf. Coat. Tech.* **343** 160-5

[3] Lee Y J, Lee C and Lee H M 2018 Synthesis of oxide-free aluminum nanoparticles for application to conductive film *Nanotechnology* **29** 055602

[4] Lynch P, Fiore G, Krier H and Glumac N 2010 Gas-phase reaction in nanoaluminum combustion *Combust. Sci. Technol.* **182** 842-57

[5] Kikawada M, Ono A, Inami W and Kawata Y 2015 Surface plasmon-enhanced fluorescence cell imaging in deep-UV region *Appl. Phys. Express* **8** 072401
[6] Taguchi A, Hayazawa N, Furusawa K, Ishitobi H and Kawata S 2009 Deep-UV tip-enhanced Raman scattering *J. Raman Spectrosc.* **40** 1324-30
[7] McClain M, Schlather A, Ringe E, King N, Liu L, A Manjavacas, M Knight, I Kumar, K Whitmire, H Everitt, P Nordlander and N Halas 2015 Aluminum nanocrystals *Nano Lett.* **15** 2751-5
[8] Honda M, Kumamoto Y, Taguchi A, Saito Y and Kawata S 2014 Plasmon-enhanced UV photocatalysis *Appl. Phys. Lett.* **104** 061108
[9] Knight M, King N, Liu L, Everitt H, Nordlander P and Halas N 2014 Aluminum for plasmonics *ACS Nano* **8** 834-40
[10] Maidecchi G, Gonella G, Zaccaria R, Moroni R, Anghinolfi L, Giglia A, Nannarone S, Mattera L, Dai H, Canepa M and Bisio F 2013 Deep ultraviolet plasmon resonance in Aluminum nanoparticle arrays *ACS Nano* **7** 5834-41
[11] Knight M, Liu L, Wang Y, Brown L, Mukherjee S, King N, Everitt H, Nordlander P and Halas N 2012 Aluminum plasmonic nanoantennas *Nano Lett.* **12** 6000-4
[12] Sanz J, Ortiz D, Osa R A, Saiz J, González F, Brown S, Losurdo M, Everitt H and Moreno F 2013 UV plasmonic behavior of various metal nanoparticles in the near- and far-field regimes: geometry and substrate effects *J. Phys. Chem.* C **117** 19606-15
[13] Tan S, Zhang L, Zhu D, Goh X, Wang Y M, Kumar K, Qiu C and Yang J 2014 Plasmonic color palettes for photorealistic printing with Aluminum nanostructures *Nano Lett.* **14** 4023-9
[14] Ekinci Y, Solak H and Löffler J 2008 Plasmon resonances of aluminum nanoparticles and nanorods *J. Appl. Phys.* **104** 083107
[15] Gérard D and Gray S 2015 Aluminium plasmonics *J. Phys.* D*: Appl. Phys.* **48** 184001
[16] Kuzma A, Weis M, Flickyngerova S, Jakabovic J, Satka A, Dobrocka E, Chlpik J, Cirak J, Donoval M, Telek P, Uherek F and Donoval D 2012 Influence of surface oxidation on plasmon resonance in monolayer of gold and silver nanoparticles *J. Appl. Phys* **112** 103531
[17] Gutierrez Y, Ortiz D, Sanz J, Saiz J, Gonzalez F, Everitt H and Moreno F 2016 How an oxide shell affects the ultraviolet plasmonic behavior of Ga, Mg, and Al nanostructures *Opt. Express* **24** 20621-31
[18] Han M, Xu C, Zhu D, Yang L, Zhang J, Chen Y, Ding K, Song F and Wang G 2007 Controllable synthesis of two-dimensional metal nanoparticle arrays with oriented size and number density gradients *Adv. Mater.* **19** 2979
[19] Hu J, Chen L, Lian Z, Cao M, Li H, Sun W, Tong N and Zeng H 2012 Deep-ultraviolet blue-light surface plasmon resonance of Al and Al-core/Al_2O_3 shell in spherical and cylindrical nanostructures *J. Phys. Chem.* C **116** 15584-90
[20] Rechberger W, Hohenau A, Leitner A, Krenn J, Lamprecht B and Aussenegg F 2003 Optical properties of two interacting gold nanoparticles *Opt. Commun.* **220** 137-41
[21] Su K, Wei Q H, Zhang X, Mock J, Smith D and Schultz S 2003 Interparticle coupling effects on plasmon resonances of nanogold particles *Nano Lett.* **3** 1087-90
[22] Gong Y, Zhou Y, He L, Xie B, Song F, Han M and Wang G 2013 Systemically tuning the surface plasmon resonance of high-density silver nanoparticle films *Eur. Phys. J.* D **67** 87
[23] Ramaswamy A and Kaste P 2005 A 'nanovision'' of the physiochemical phenomena occurring in nanoparticles of aluminum *J. Energ. Mater.* **23** 1-25
[24] Levitas V, McCollum J and Pantoya M 2015 Pre-stressing micron-scale Aluminum core-shell particles to improve reactivity *Sci. Rep.* **5** 7879